Deep Transfer Learning-Based Demagnetization Analysis for Linear Oscillating Actuator Considering Circumferential Segmented Structure

Ji-Hyeon Lee, Soo-Hwan Park, *Member, IEEE*, Du-Ha Park, Jae-Hoon Jeong, and Myung-Seop Lim, *Senior Member, IEEE*

***Abstract*—This article proposes a method for estimating the 3-D FEA-based demagnetization ratio (DR), which serves as a key measure for assessing irreversible demagnetization, using deep transfer learning. The complex configuration of the LOA, such as the segmented outer stator and permanent magnets (PMs), reduces the accuracy of 2-D axisymmetric finite element analysis (FEA). While 3-D FEA provides a more precise DR estimation, its substantial computational cost poses a significant challenge. Therefore, we propose a deep transfer learning-based demagnetization analysis method that improves computational efficiency while preserving high accuracy. This approach takes into account the permeance in the stator core and circumferential leakage flux. By leveraging deep transfer learning, knowledge acquired from a large-scale 2-D axisymmetric FEA-based DR dataset is transferred to a limited 3-D FEA-based DR dataset, effectively enhancing deep neural network performance. The DR predicted by the proposed method was compared with the results obtained from 3-D FEA. Using the proposed method, the analysis time is significantly reduced compared to employing only 3-D FEA, while maintaining high accuracy. This demonstrates its potential for accurate and efficient demagnetization analysis, positioning it as a viable solution for LOA design optimization. The proposed method is validated through computer simulations and experiments under various demagnetization conditions.**

***Index Terms*—Deep neural network, demagnetization ratio, finite element analysis, linear oscillating actuator, transfer learning.**

Received 3 February 2025; revised 9 May 2025; accepted 6 June 2025. Date of publication 2 July 2025; date of current version 22 January 2026. Paper 2024-EMC-1783.R1, presented at the 2023 IEEE Transportation Electrification Conference and Expo, Asia-Pacific, Chiang Mai, Thailand, Nov. 28–Dec. 01, and approved for publication in the IEEE TRANSACTIONS ON INDUSTRY APPLICATIONS by the Electric Machines Committee of the IEEE Industry Applications Society [DOI: 10.1109/ITECAsia-Pacific59272.2023.10372241]. *(Corresponding author: Myung-Seop Lim.)*

Ji-Hyeon Lee and Du-Ha Park are with the Department of Automotive Engineering (Automotive Computer Convergence), Hanyang University, Seoul 04763, South Korea (e-mail: jigus@hanyang.ac.kr; yjmkdoo@hanyang.ac.kr).

Soo-Hwan Park is with the Department of Mechanical, Robotics and Energy Engineering, Dongguk University, Seoul 04620, South Korea (e-mail: parksh@dgu.ac.kr).

Jae-Hoon Jeong is with H&A Fundamental Technology R&D Lab, LG Electronics, Seoul 08592, South Korea (e-mail: jaehoon02.jeong@lge.com).

Myung-Seop Lim is with the Department of Automotive Engineering, Hanyang University, Seoul 04763, South Korea (e-mail: myungseop@hanyang.ac.kr).

Color versions of one or more figures in this article are available at https://doi.org/10.1109/TIA.2025.3585098.

Digital Object Identifier 10.1109/TIA.2025.3585098

I. Introduction

LINEAR oscillating actuator (LOA) provides linear oscillatory thrust force directly without using a special mechanism such as a crank shaft to convert rotary motion to linear oscillations [1]. This direct operation eliminates mechanical losses and improves overall system efficiency, making the LOA an attractive solution for various applications. Due to its high power density, efficiency, and compact structure, the LOA has gained significant attention in industries requiring precise linear motion [2]. It is widely utilized in devices such as compressors, linear pumps, and automobile active suspension systems, where reliable and efficient oscillatory motion is essential [3], [4], [5]. Additionally, advancements in materials and control strategies have further enhanced the performance and applicability of LOAs in modern engineering systems.

The stability of permanent magnets (PMs) is crucial for maintaining the electromagnetic performance of LOAs, as various factors—including temperature fluctuations, external electromagnetic fields, and design parameters such as magnet thickness and length—can influence their stability. These factors affect the load line or the PMs B-H curve, both of which determine the operating point on the B-H curve. If the operating point shifts below the knee point due to excessive temperature rise or strong electromagnetic interference, irreversible demagnetization occurs, leading to a permanent loss of magnetic properties and degraded system performance [6], [7]. Since irreversible demagnetization significantly impacts the thrust force characteristics of LOAs, accurately predicting and preventing such occurrences is essential for ensuring long-term reliability. Unlike conventional radially symmetric PMSMs, the LOA investigated in this study incorporates a segmented outer stator and segmented permanent magnets, resulting in circumferential flux leakage and local magnetic saturation. These structural characteristics significantly affect the probability of irreversible demagnetization, which must be accurately predicted to avoid overdesign. Therefore, it is essential to consider demagnetization in the LOA design process. Moreover, in specific motor types, such as line-start PMSMs, which experience high asynchronous starting currents, or machines employing low-coercivity magnets, the risk of demagnetization is inherently higher [8], [9]. Consequently, considering demagnetization effects at the design stage is essential for ensuring reliable operation in such configurations.

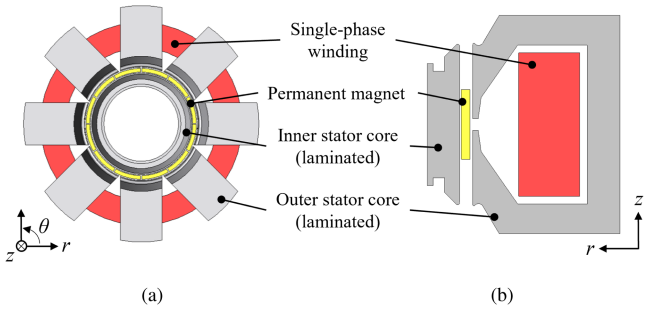

Fig. 1. Analysis model of the LOA. (a) 3-D FEA. (b) 2-D axisymmetric FEA.

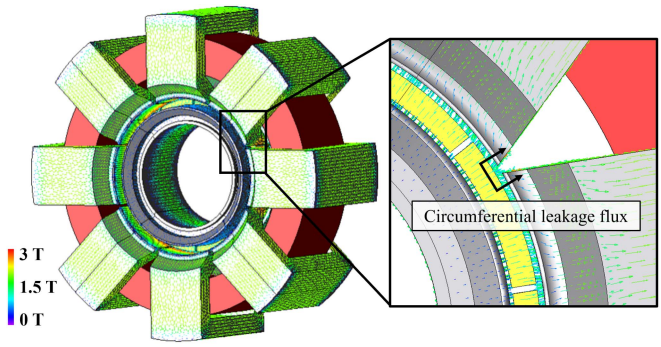

Fig. 2. Circumferential flux leakage path at the outer stator from 3-D FEA results of the LOA.

As a result, studies have been conducted to incorporate demagnetization effects into the design process, aiming to enhance the reliability and performance of motor [10], [11].

Fig. 1 shows the structure of an LOA, which consists of outer and inner stators, a single-phase winding and PMs. When a sinusoidal current is applied to the stator winding, an alternating magnetic field is generated, which establishes a time-varying magnetic flux path through the stator core, the air gap, and the PMs. As the flux density changes over time, it interacts with the PMs to produce an axial electromagnetic thrust force. This force is primarily governed by Maxwell stress and magnetic reluctance variation [12]. Because the excitation current oscillates sinusoidally, the direction of the electromagnetic force alternates correspondingly, resulting in a periodic reciprocating motion of the mover along the axial axis. The magnitude and dynamics of this motion are determined by the amplitude and frequency of the input current, the geometry of the LOA, and the magnetic properties of the materials.

The inner and outer stators are laminated to reduce the iron loss. Unlike the inner stator, the outer stator and PMs are divided into several pieces owing to manufacturing constraints. The air regions created by the segmented outer stator structure can cause magnetic saturation that affects the electromagnetic performance of the LOA. This occurs because the absence of ferromagnetic material in air regions allows more magnetic flux to pass through the segmented outer stator [13], [14]. Fig. 2 presents the circumferential flux leakage path at the outer stator obtained from the 3-D FEA results of the LOA. This flux leakage phenomenon significantly affects the magnetic flux distribution

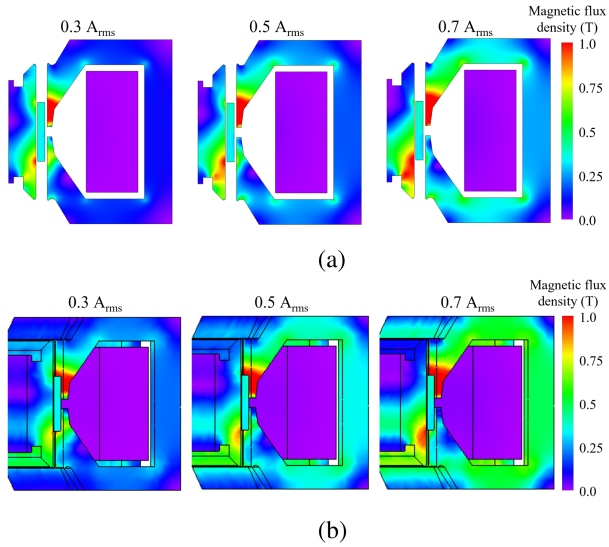

Fig. 3. Contour plot of magnetic flux density. (a) 2-D axisymmetric FEA (b) 3-D FEA.

and saturation levels in the stator. Furthermore, the segmented PM structure affects magnetic flux distribution, which varies depending on magnet utilization [15]. The segmented structure of the outer stator and PMs creates a complex flux path that 2-D axisymmetric analysis cannot accurately model, as it assumes a solid core structure instead of a segmented core. Fig. 3 shows the contour plot of the magnetic flux density obtained from both 2-D axisymmetric FEA and 3-D FEA. In Fig. 3(a), the 2-D axisymmetric FEA results exhibit an oversimplified flux distribution due to the assumption of axial symmetry. This approach neglects the effects of flux leakage and segmentation, leading to an inaccurate prediction of saturation regions. In contrast, Fig. 3(b) presents the results from 3-D FEA, where the actual flux distribution, including leakage and saturation effects, is represented more accurately. The discrepancy between these two methods highlights the necessity of 3-D FEA for a accurate electromagnetic performance analysis.

In order to calculate the performance of LOA, 2-D axisymmetric FEA is required to reduce the computation cost rather than using the 3-D FEA. However, 2-D axisymmetric FEA for electromagnetic field analysis cannot guarantee accuracy when analyzing LOA with complex structure of outer stator and PMs. This is because the effects of the magnetic flux distribution changes cannot be considered in 2-D axisymmetric FEA [16]. Thus, accurate demagnetization ratio (DR) which is the factor that determine occurrence of the irreversible demagnetization can only be calculated by using 3-D FEA, resulting in high computational cost for the design process of LOA [17]. Therefore, accurate cost-effective method for calculating the DR of the LOA is required.

Thus, in this paper, we propose a computationally efficient analysis method for calculating DR of the LOA only using deep transfer learning. This method reduces the computational cost while improving the accuracy of DR calculations through the following steps. First, sampling points are derived through a Design of Experiments (DOE), and demagnetization analysis

are conducted for each sampling point in both 2-D axisymmetric and 3-D FEA. Second, the first deep neural network (DNN) for predicting 2-D axisymmetric FEA-based DR is trained with a large amount of 2-D axisymmetric FEA-based DR. Third, the second DNN for predicting 3-D FEA-based DR is trained with a small amount of 3-D FEA-based DR with deep transfer learning. Subsequently, the DR can be predicted using the second DNN according to the factors that affects irreversible demagnetization. With the proposed method, accurate and more cost-effective DR calculations can be performed using a large amount of 2-D axisymmetric FEA data, which has a low computational cost, combined with a small amount of 3-D FEA data, which has a high computational cost, than using only a large amount of 3-D FEA data. This paper presents a computationally efficient predictive framework that leverages deep transfer learning to estimate demagnetization-related responses obtained from FEA across a wide range of design variables. The proposed approach is particularly effective during the early stages of design, where rapid evaluation and identification of high-risk demagnetization regions are essential to achieve reliable and optimized LOA performance. By transferring knowledge from a large-scale 2-D FEA dataset to a limited 3-D FEA dataset, the framework significantly reduces computational cost while maintaining high prediction accuracy. This enables efficient exploration of the LOA design space under various operating conditions, including changes in armature current, PM temperature, PM position, and design variables. Therefore, to predict the DR of the LOA using deep transfer learning, a previous study, presented at the 2023 IEEE Conference and Expo Transportation Electrification Asia-Pacific (ITEC Asia-Pacific), had proposed a method that considers both the circumferential flux leakage of 3-D FEA and the relatively fast computational time of axisymmetric FEA [18].

The organization of this article is as follows. Section II: Demagnetization: Principles and Analytical Methods describes demagnetization principles and how the demagnetization analysis is conducted for the LOA, including the method used to evaluate the DR. Section III: Demagnetization Analysis Based on Deep Transfer Learning presents the methodology for performing demagnetization analysis using deep transfer learning. Section IV: Experimental Verification discusses the demagnetization experiments conducted on 8 prototypes to verify the results. Finally, the conclusions of the study are presented in Section V: Conclusion.

II. Demagnetization: Principles and Analytical Methods

A. Demagnetization: Principles

Fig. 4(a) and (b) shows the demagnetization characteristic curve. Fig. 4(a) shows the relationship between the permeance coefficient and the operating point of the PM. The stability of magnetic materials is determined by their resistance to demagnetization, which is characterized by the maximum energy product $B - H_{\max}$, defined by the recoil line of the B-H demagnetization curve. This energy product indicates the maximum energy the magnet can store before losing its magnetization. The magnet's operating flux density B_m and the magnetic field intensity H_m

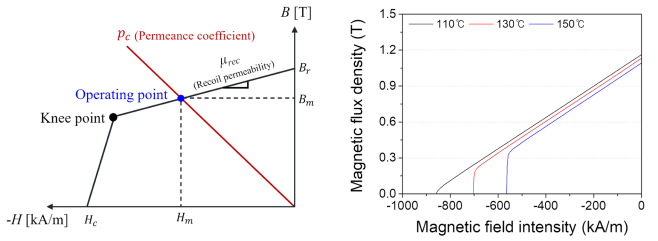

Fig. 4. Demagnetization characteristic curve. (a) Permeance coefficient and the operating point. (b)Temperature-dependent demagnetization characteristic curve.

are critical for the magnet's performance and susceptibility to demagnetization. Operating near the knee point on the B-H curve increases the risk of demagnetization, and for stable operation, the magnet must be kept above this point. If the operating point falls below the knee point, irreversible demagnetization occurs, leading to a permanent loss of magnetization.

The operating point is defined by the intersection of the demagnetization curve and the load line of the PM [19]. The permeance coefficient p_c, which is the load line slope, can expressed as follows:

$$p_c = \frac{B_m}{\mu_0 |H_m|} = \frac{1}{f_{lkg}} \cdot \frac{l_{\mathrm{PM}}}{l_{\mathrm{g}}} \cdot \frac{A_g}{A_m} \tag{1}$$

where μ_0 is the vacuum permeability, B_m and H_m represent the magnetic flux density and magnetic field at the operating point, respectively. Additionally, f_{lkg} denotes the leakage coefficient, while l_{PM} and l_{g} represent the PM thickness and air-gap length, respectively. A_g and A_m correspond to the axial cross-sectional areas per pole of the air-gap and PM, respectively. The point of intersection between the magnet's B-H curve and the load line is the operating point of the magnet. The load line represents the magnet's operating conditions, and its position relative to the demagnetization curve determines whether demagnetization will be reversible or irreversible. If the operating point is below the knee point, irreversible demagnetization is inevitable.

Main factors influencing demagnetization include temperature, external demagnetizing fields, and the PM's load line [20]. When external demagnetizing fields exceed a threshold, irreversible demagnetization takes place, and the magnet follows the recoil line, permanently losing its magnetic properties. To prevent this, the magnet must operate above the knee point, and it is important to consider this during the design stage.

B. Demagnetization: Analytical Methods

The specifications of the LOA are listed in Table I. PMs demagnetization in LOA is treated as a critical phenomenon in which a magnet loses its ability to generate a magnetic flux partially. Fig. 5 shows the description of the demagnetization analysis input parameters and their parameter ranges. The operating point can fall from the knee point of the B-H curve with the external influence, such as temperature rise, armature current and PM position at load, resulting in an irreversible demagnetization [21]. Additionally, the thickness and length

TABLE I
SPECIFICATIONS OF LOA BASE MODEL

Item	Unit	Value
Stroke	mm	11
Output power	W	61.69
Outer stator outer radius	mm	73.45
Inner stator outer radius	mm	31.7
PM length	mm	18
PM thickness	mm	3
Inner stator core material	-	50PN470
Outer stator core material	-	35PN230

Parameter	Unit	*Min value*	*Max value*
PM thickness	mm	1	4
PM length	mm	10	29
Demag. PM position	mm	0	11
Demag. temperature	°C	110	150
Demag. current	A	0	7

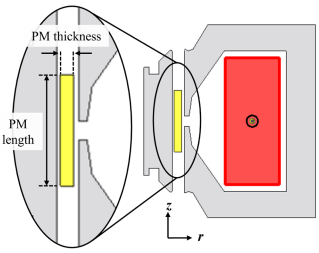

Fig. 5. Description of demagnetization analysis input parameters.

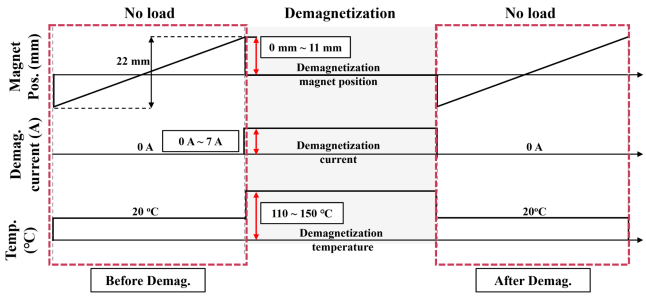

Fig. 6. Procedure of the LOA demagnetization analysis.

of the PM are also important factors, leading to irreversible demagnetization [22]. Furthermore, the length of the magnet can affect the LOA flux path and saturation, which can shift the operating point and influence demagnetization. Therefore, in this study, the parameters considered for the analysis were magnet thickness, magnet length, temperature, demagnetizing current, and magnet position.

Fig. 6 shows the procedure of the LOA demagnetization analysis. The procedure of the LOA demagnetization analysis is carried out as follows:

1) The PM position moves linearly from −11 mm to 11 mm at a speed of 1 m/s while analyzing the Back Electro Motive Force (Back-EMF). During this process, the demagnetization temperature is set to 0 °C, and the demagnetizing current is 0 A. The Back-EMF during this stage is referred to as the Back-EMF before demagnetization.
2) The PM position is fixed at a specific value, and a particular demagnetization temperature and demagnetizing current are applied. The conditions are the same as shown in Fig. 4, and under these conditions, the magnet undergoes partial demagnetization.

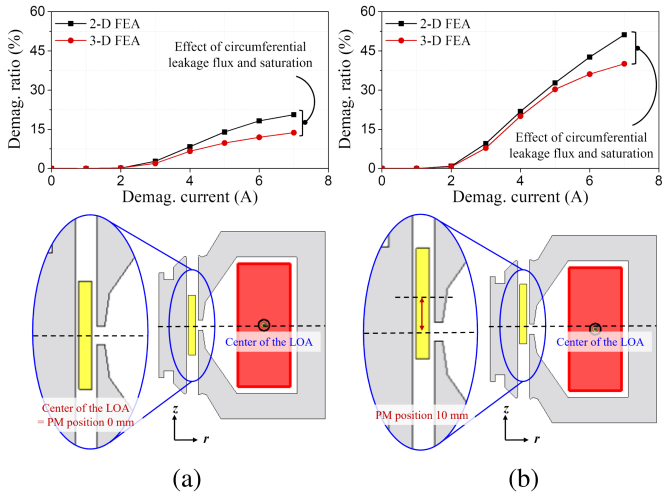

Fig. 7. Comparison of 2-D axisymmetric and 3-D FEA-based demagnetization ratio according to armature current. (a) $PM_{pos.} = 0$ mm. (b) $PM_{pos.} = 10$ mm.

3) The PM position moves linearly from −11 mm to 11 mm at a speed of 1 m/s while analyzing the Back-EMF. During this process, the demagnetization temperature is set to 0 °C, and the demagnetizing current is 0 A. The Back-EMF in this stage is referred to as the Back-EMF after demagnetization.

When the PM irreversible demagnetization occurs, the residual magnetic flux density of PM is permanently decrease. Therefore, the Back-EMF amplitude will change. To determine the occurrence of the irreversible demagnetization, a DR is introduced in this article. The DR is expressed as

$$\mathrm{DR}(\%) = \frac{E_{before} - E_{after}}{E_{before}} \times 100 \tag{2}$$

where E_{before} is the Back-EMF before demagnetization and E_{after} is the Back-EMF after demagnetization.

Fig. 4(b) shows the temperature-dependent demagnetization characteristic curve, which was used in the analysis. Fig. 7 shows the comparison of DR obtained from 2-D axisymmetric and 3-D FEA based on the armature current. Fig. 7(a), with PM position at 0 mm, and Fig. 7(b), with PM position at 10 mm, show the differences in DR between the two methods. The difference between the LOA center and the PM center is defined as the PM position. These differences are primarily due to the effects of circumferential leakage flux and magnetic saturation, which are accounted for in the 3-D FEA but are not considered in the 2-D axisymmetric FEA. The results from 3-D FEA exhibit notable variations in DR because of these factors, which are crucial for accurately predicting the demagnetization behavior of the LOA.

III. DEMAGNETIZATION ANALYSIS BASED ON DEEP TRANSFER LEARNING

A. Deep Transfer Learning

A deep neural network (DNN) is widely used as a surrogate model for predict motor performance because it shows excellent

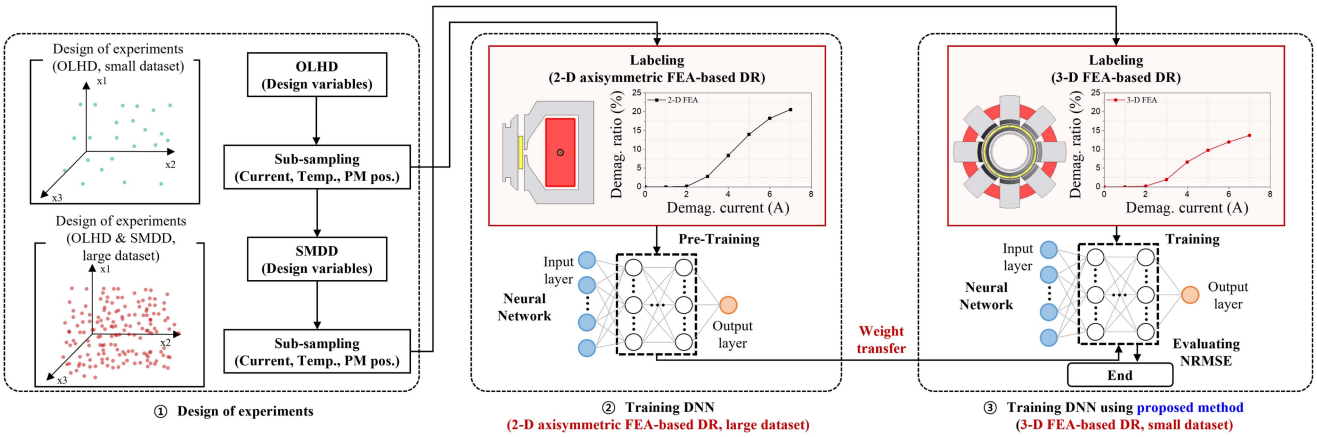

Fig. 8. Flowchart for proposed deep transfer learning-based DR prediction.

performance on various tasks such as regression or classification [23], [24]. Generally, a large amount of data is required to achieve high performance of DNN. Therefore, applications such as regression of electromagnetic performance using 3-D FEA require a lot of computing resources to obtain high performance of DNN. Transfer learning is a technique that takes domain knowledge of a pre-trained model for the multi dimensional source dataset, $X^s \in R^{n\times p}$, and used it to train a new model for the target dataset, $X^t \in R^{n\times p}$, with n denoting the number of observations and p denoting the number of input feature [25]. It can be effectively used when DNN cannot be trained sufficiently because it is difficult to obtain the label of the target dataset. The principle of transfer learning is as follows. Assume that the source and target datasets have similar distributions but have bias. The source dataset has a relatively large size compared with the target dataset because it is relatively easy to obtain labels compared with the target dataset. The source DNN has high regression performance because it is trained to follow the data distribution of the source dataset. Therefore, to use the domain knowledge of the source model that has a similar distribution to the target dataset, the layers of the target DNN except for several top layers are transferred from the pre-trained layers of the source model. The comparison of 2-D axisymmetric FEA and 3-D FEA-based DR according to armature current as shown in Fig. 7(a) and (b). 2-D axisymmetric FEA-based DR and 3-D FEA-based FEA DR have similar distributions but have bias. Also, it is more difficult to obtain the label of the 3-D FEA-based DR than that of the 2-D axisymmetric FEA-based DR. Therefore, 2-D axisymmetric FEA-based DR can be seen as a source dataset and 3-D FEA-based DR can be seen target dataset.

B. Proposed Demagnetization Analysis

Fig. 8. shows a process for the proposed deep transfer learning-based prediction DR. In this study, the target output of the DNN is the DR, which is calculated using the procedure described in Section II-B. To train the model, a labeled dataset is constructed using the demagnetization analysis method based on FEA described earlier. Specifically, the input parameters such as current, temperature, PMs position and design variables are sampled through a DOE strategy, and the resulting DR is calculated using JMAGDesigner simulations.

The DOE is the sampling plan in the input design variable or parameter domain. In this paper, the Optimal Latin Hypercube Design (OLHD) was used to generate the small dataset for 3-D FEA [26], [27]. Additionally, the Sequential Maximin Distance Design (SMDD) was employed to generate the large dataset for 2-D axisymmetric FEA. The goal of the SMDD is to select new samples from unexplored regions of the design space. The selection process of these new samples is based on the initial samples generated using the OLHD. New samples are then chosen as points that maximize the minimum average distance from the labeled samples [28]. Subsequently, sub-sampling is performed at each design variable sampling point—focusing on parameters such as armature current, PM temperature, and PM position—and an electromagnetic analysis is conducted for each derived experimental point. Although DOE is commonly used in design optimization studies, in this work, it is employed purely as a sampling tool for training data generation, and not for solving an optimization problem.

The 2-D axisymmetric FEA-based DR can be acquired faster than 3-D FEA-beased DR, and each DR has a similar data distribution. Therefore, DNNs are trained by transfer learning with 2-D axisymmetric-based dataset as a source data and the 3-D FEA-based dataset as a target data for considering circumferential leakage flux and complex structure of the LOA. After training DNNs, the DR according to the desired demagnetization-related are predicted through DNNs. The source and target data were labeled using JMAG, a commercial FEA software, after DOE based on OLHD and SMDD. The input features range are presented in Fig. 5. For each sample, the labeling process was conducted by calculating DR according to armature current, PM temperature and PM position which affect irreversible demagnetization of PM. The DNN is for predicting DR which is affected by magnetic saturation and circumferential leakage flux.

C. Learning Performance With Deep Transfer Learning

The structure of DNN was determined through the hyperparameter tuning process. The hyperparameters are tunable parameters that allow us to control the training process of deep

TABLE II
DETAILED SETTING OF DNN

Item	Value
Number of layers	4
Number of units	256
Learning rate	5e-3
Activation function	ReLU
Optimizer	Adam
Loss function	Mean squared error
Size of mini-batch	16

learning model. As the performance of the model is highly dependent on the combination of hyperparameters, the process for hyperparameter tuning is necessary. The architecture of DNN was selected as a multi-layer perceptron (MLP). The perceptron is an algorithm that mimics the priciple of biological neuron, which gives the sum of multiple inputs multiplied by weights. MLP is a structure in which layers, a set of perceptrons, are stacked and is generally used for pattern recognition of complex dataset. The detailed setting of DNN are listed in Table II. The number of the source dataset was 10 times larger than that of the target datasets. The hyperparameters of DNN was selected as the number of hidden layers and units, and the learning rate for Adam optimizer. To avoid overfitting, the source dataset was split into training, validation and test datasets at a ratio of 8:1:1 [29], [30]. As a result of hyperparameter tuning, the number of layers, units, and learning rate was selected as 4, 256 and 5e-3 respectively. The target DNNs were trained using transfer learning, and training was conducted by transferring the weights of four layers among the four hidden layers. The target dataset was split into training and validation datasets at a ratio of 9:1. The target DNN and the transferred weights are re-optimized to retain the knowledge transferred from the source DNN as follows [31]:

$$\min_{w} L(w) = \frac{1}{n}\sum_{i=1}^{n}(y_i - \hat{y}_i)^2 \tag{3}$$

where L is the loss function, n is the number of target datasets, and y_i and $\hat{y}_i$ denote the ground truth and the predicted value from the neural network, respectively.

The learning curves of the source DNNs and target DNNs with or without transfer learning are shown in Fig. 9(a) and (b). The mean squared error (MSE) values of a large amount of the 2-D axisymmetric FEA-based DR dataset and a small amount of the 3-D FEA-based DR with transfer leaning are low, it can be seen that both of DNNs were well trained. As opposed to DNNs with transfer leaning, The MSE values of DNNs with a large amount of the 3-D FEA-based DR without transfer learning is higher. Fig. 10 shows the comparison between prediction and ground truth with and without transfer learning for the test dataset. The normalized MSE for each case is 0.18% and 10.00%, respectively, indicating that predictions using deep transfer learning achieve higher accuracy. As a result of using transfer learning, it can be seen that the regression performance was highly well-evaluated, and as a result of DNNs with a large amount

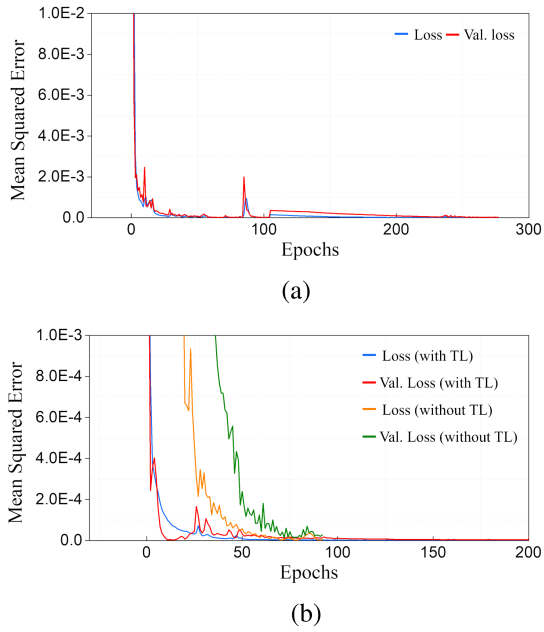

Fig. 9. Learning curve. (a) 2-D axisymmetric FEA-based DR. (b) 3-D FEA-based DR with and without transfer learning.

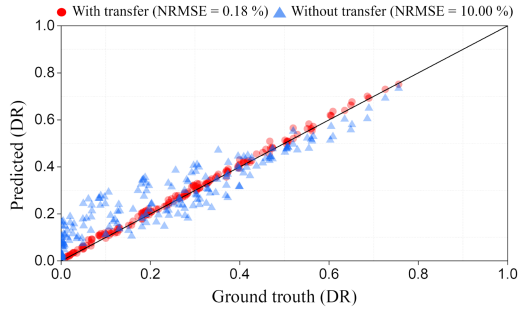

Fig. 10. Comparison between ground truth and prediction with or without transfer learning for test dataset.

of the 3-D FEA-based DR without transfer learning, it can be seen that the regression performance was degraded. Therefore, high regression performance can be achieved using transfer learning with a small amount of 3-D FEA data. Fig. 11(a)–(c) shows comparison of DR between 2-D axisymmetric, 3-D FEA and results using the proposed method, demonstrating that the proposed method produces results closely matching those of 3-D FEA. Fig. 11(a) shows the DR values for PM positions of 0 mm, 2.75 mm, 5.5 mm, and 8.25 mm from left to right, given a magnet thickness of 2.93 mm, a magnet length of 10.91 mm, and demagnetization temperature of 150 °C. Fig. 11(b) shows the DR values for PM positions of 0 mm, 2.75 mm, 5.5 mm, and 8.25 mm from left to right, given a magnet thickness of 3.99 mm, a magnet length of 19.68 mm, and demagnetization temperature of 130 °C. Fig. 11(c) shows the DR values for PM positions of 0 mm, 2.75 mm, 5.5 mm, and 8.25 mm from left to right, given a magnet thickness of 1.40 mm, a magnet length of 26.43 mm, and demagnetization temperature of 110 °C. The DR difference between the 3-D FEA and the proposed method is a maximum of 1.83%, demonstrating that the results

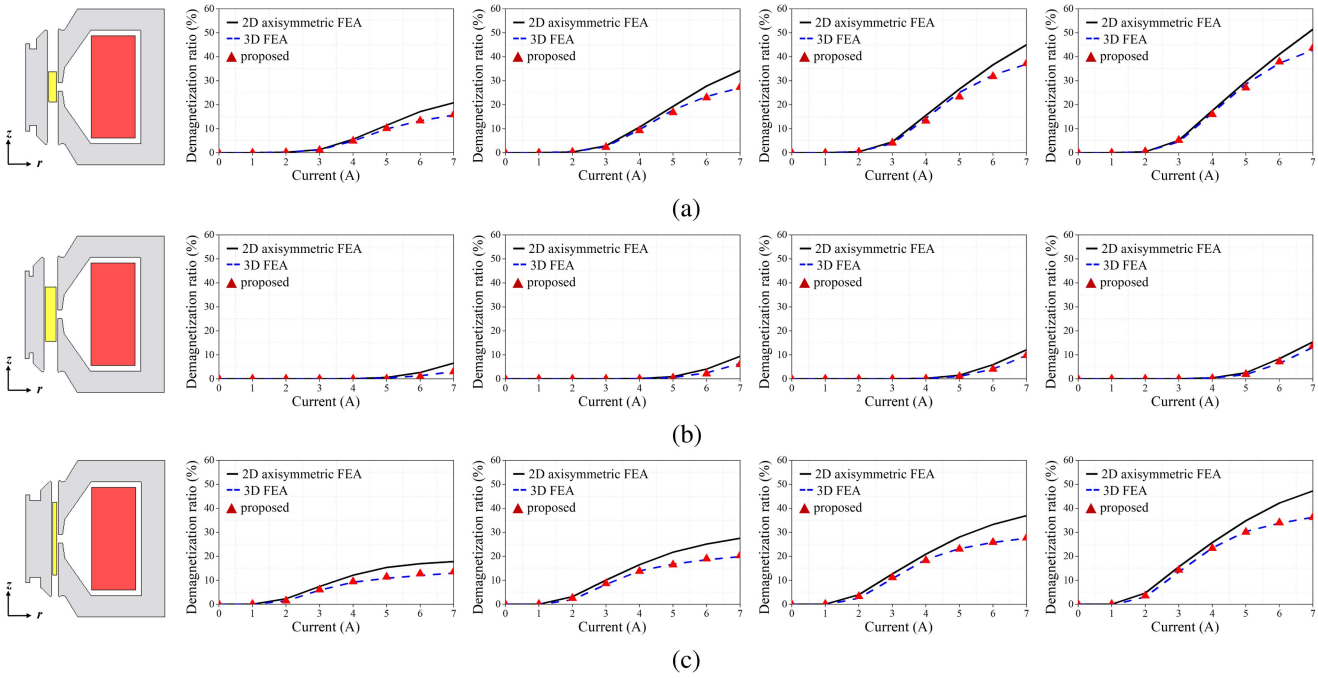

Fig. 11. Comparison of DR between 2-D axisymmetric, 3-D FEA and results using the proposed method. (a) Sample point 1. (b) Sample point 2. (c) Sample point 3.

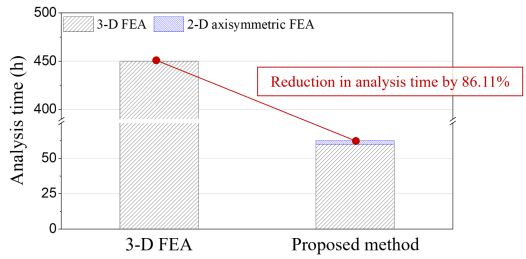

Fig. 12. Comparison of DR between 3-D FEA and results using the proposed method.

obtained from the proposed method are in good agreement with those from the 3-D FEA. Fig. 12 shows comparison of DR between 3-D FEA and results using the proposed method. It also illustrates the analysis time for 2-D axisymmetric and 3-D FEA when applying the proposed method, as well as the analysis time for 3-D FEA without the proposed method. The results indicate that applying the proposed method achieves an 86.11% reduction in computational time.

IV. Experimental Verification

The proposed method utilizes transfer learning to predict the demagnetization ratio, which is calculated using 3-D FEA. The base model was realized and experimental validation was conducted. Fig. 13(a)–(d) illustrate the experimental setups corresponding to the sequence of the demagnetization experiment. A total of 8 specimens were fabricated, each subjected to experiments under different conditions, including varying temperature, PM position, and current. The experiment was conducted in the following sequence:

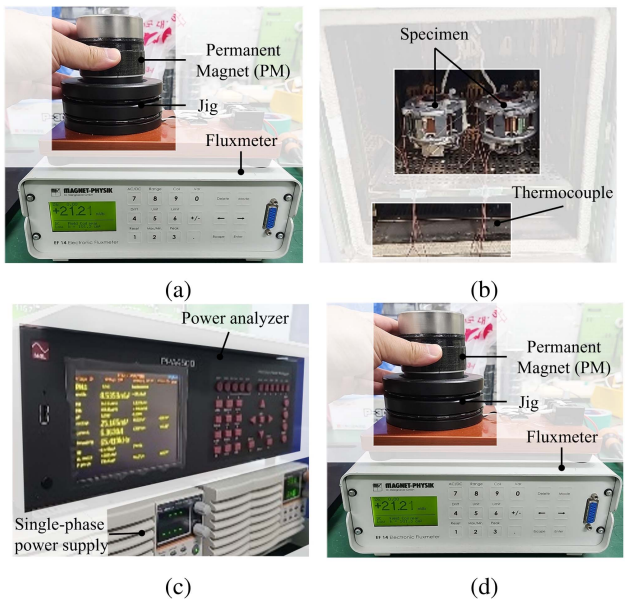

Fig. 13. Comparison of 2-D axisymmetric and 3-D FEA-based demagnetization ratio according to armature current. (a) $PM_{pos.} = 0$ mm. (b) $PM_{pos.} = 10$ mm.

1) The first step in the experiment involves measuring the magnetic flux of the specimen before the demagnetization process. The specimen is placed in a magnetic field measurement system, and the magnetic flux is captured using a fluxmeter. The specimen is stabilized at room temperature for 12 hours to ensure a consistent initial condition. This period of stabilization is crucial to minimize any environmental variations that may affect the magnetic

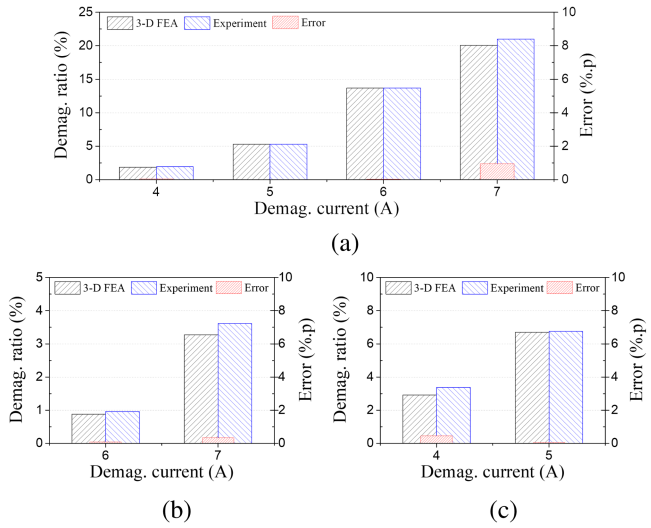

Fig. 14. Comparison of DR between experimental results and 3-D FEA. (a) DR at 115 °C and PM $_{pos.}$ = 11 mm. (b) DR at 115 °C and PM $_{pos.}$ = 0 mm. (c) DR at 130 °C and PM$_{pos.}$ = 0 mm .

flux measurements. Fig. 13(a) illustrate the experimental setups for flux measurement.

2) Following the initial magnetic flux measurement, the specimen is subjected to heating in a temperature-controlled chamber. The chamber is designed to precisely control the temperature of the specimen, ensuring a gradual increase in temperature to reach the target value. A thermocouple is installed on the specimen's surface to monitor the temperature in real time and ensure uniform temperature distribution across the specimen. Fig. 13(b) illustrate the experimental setups of temperature-controlled chamber. Once the specimen reaches the target temperature, a direct current (DC) is applied through a power supply. Fig. 13(c) illustrate the experimental setups for applying DC. Throughout this phase, the power analyzer measures the electrical power and current, which are continuously monitored to maintain proper parameters for the demagnetization process.
3) After the specimen has been subjected to the DC current for a predetermined duration, it is disconnected from the power supply. The specimen is then allowed to cool to room temperature. The final step involves re-measuring the magnetic flux, and this post-demagnetization measurement is compared with the initial magnetic flux measurement to assess the extent of demagnetization. Fig. 13(d) illustrates the magnetic flux measurement setup following the demagnetization process.

In this section, The DR is expressed as

$$\mathrm{DR}(\%) = \frac{\Phi_{before} - \Phi_{after}}{\Phi_{before}} \times 100 \tag{4}$$

where Φ_{before} is the flux before demagnetization and Φ_{after} is flux after demagnetization.

Fig. 14(a)–(c) show the comparison between the experimental and 3-D FEA results for all 8 specimens, each under different conditions. In Fig. 14(a), the DR is analyzed at a temperature of 115 °C and a PM position of 11 mm, with a demagnetization current ranging from 4 to 7 A. Fig. 14(b) presents the DR at the same temperature 115 °C, but with the PM positioned at 0 mm and a demagnetization current ranging from 6 to 7 A. Finally, Fig. 14(c) compares the DR at a higher temperature of 130 °C and a PM position of 0 mm, with a demagnetization current ranging from 4 to 5 A. The relative error between the experimental DR and the 3-D FEA DR was less than 0.94% p.

V. Conclusion

Accurate calculation of DR requires high computational costs since 3-D FEA is essential for considering the circumferential leakage flux and complex structure of LOA. Thus, in this paper, computationally efficient analysis of deep transfer learning-based DR considering the segmented mover and outer stator structure and circumferential leakage flux of the LOA was proposed. First, label the 2-D axisymmetric FEA-based DR and 3-D FEA-based DR dataset by using DOE and sub-sampling. Second, pre-train the model using 2-D axisymmetric FEA-based DR data. Finally, use the knowledge from the pre-trained model to train the small amount of 3-D FEA-based DR data. The results show that the proposed method allows for fast and accurate learning even with a small amount of 3-D FEA data. In addition, experimental verification is presented to verify the proposed method. By using the proposed method, the irreversible demagnetization of the LOA can be accurately estimated at the design stage because the magnetic flux density increased according to the LOA structure and circumferential leakage flux are considered via proposed method, and the computation cost can be reduced when designing a LOA. Furthermore, the proposed method is adaptable and can be effectively utilized in the design of other LOA with varying dimensions.

References

[1] C.-W. Kim et al., "Comparison of electromagnetic and dynamic characteristics of linear oscillating actuators with rare-earth and ferrite magnets," *IEEE Trans. Magn.*, vol. 55, no. 7, Jul. 2019, Art. no. 8203204, doi: 10.1109/TMAG.2018.2890025.
[2] Z. Q. Zhu and X. Chen, "Analysis of an E-core interior permanent magnet linear oscillating actuator," *IEEE Trans. Magn.*, vol. 45, no. 10, pp. 4384–4387, Oct. 2009, doi: 10.1109/TMAG.2009.2022049.
[3] I. Martins, J. Esteves, G. D. Marques, and F. Pina da Silva, "Permanent-magnets linear actuators applicability in automobile active suspensions," *IEEE Trans. Veh. Technol.*, vol. 55, no. 1, pp. 86–94, Jan. 2006, doi: 10.1109/TVT.2005.861167.
[4] Z. Ahmad, A. Hassan, F. Khan, N. Ahmad, B. Khan, and J. Ro, "Analysis and design of a novel outer mover moving magnet linear oscillating actuator for a refrigeration system," *IEEE Access*, vol. 9, pp. 121240–121252, 2021, doi: 10.1109/ACCESS.2021.3109068.
[5] H. Zhang et al., "Detent force reduction design for the C-core single-phase permanent magnet linear oscillation actuator," *IEEE Trans. Ind. Appl.*, vol. 59, no. 2, pp. 1577–1587, Mar./Apr. 2023, doi: 10.1109/TIA.2022.3225369.
[6] S. Ruoho, J. Kolehmainen, J. Ikaheimo, and A. Arkkio, "Interdependence of demagnetization, loading, and temperature rise in a permanent-magnet synchronous motor," *IEEE Trans. Magn.*, vol. 46, no. 3, pp. 949–953, Mar. 2010, doi: 10.1109/TMAG.2009.2033592.
[7] G. Mörée, J. Sjölund, and M. Leijon, "A review of permanent magnet models used for designing electrical machines," *IEEE Trans. Magn.*, vol. 58, no. 11, Nov. 2022, Art. no. 2102719, doi: 10.1109/TMAG.2022.3200150.

[8] K. A. Hadi and M. Baghayipour, "A new structure for line-start non-slotted axial-flux permanent magnet motor, proposing a novel 3D FEA-based demagnetization reduction approach," *COMPEL-Int. J. Computation Math. Elect. Electron. Eng.*, vol. 42, no. 6, pp. 1225–1247, 2023.
[9] A. Vagati, B. Boazzo, P. Guglielmi, and G. Pellegrino, "Design of ferrite-assisted synchronous reluctance machines robust toward demagnetization," *IEEE Trans. Ind. Appl.*, vol. 50, no. 3, pp. 1768–1779, May/Jun. 2014.
[10] Y.-H. Jung, M.-R. Park, K.-O. Kim, J.-W. Chin, J.-P. Hong, and M.-S. Lim, "Design of high-speed multilayer IPMSM using ferrite PM for EV traction considering mechanical and electrical characteristics," *IEEE Trans. Ind. Appl.*, vol. 57, no. 1, pp. 327–339, Jan./Feb. 2021, doi: 10.1109/TIA.2020.3033783.
[11] N. Bianchi and H. Mahmoud, "An analytical approach to design the PM in PMAREL motors robust toward the demagnetization," *IEEE Trans. Energy Convers.*, vol. 31, no. 2, pp. 800–809, Jun. 2016, doi: 10.1109/TEC.2016.2523556.
[12] Z. Q. Zhu and X. Chen, "Analysis of an E-core interior permanent magnet linear oscillating actuator," *IEEE Trans. Magn.*, vol. 45, no. 10, pp. 4384–4387, Oct. 2009.
[13] T. Wang et al., "Analytical modeling of linear oscillating motor with a mixed method considering saturation effect," *Sensors Actuators A, Phys.*, vol. 234, pp. 375–383, 2015.
[14] F. Poltschak and P. Ebetshuber, "Design of integrated magnetic springs for linear oscillatory actuators," *IEEE Trans. Ind. Appl.*, vol. 54, no. 3, pp. 2185–2192, May/Jun. 2018, doi: 10.1109/TIA.2018.2800681.
[15] K. H. Kim, H. I. Park, S. S. Jeong, S. M. Jang, and J. Y. Choi, "Comparison of characteristics of permanent-magnet linear oscillating actuator according to laminated method of stator core," *IEEE Trans. Appl. Supercond.* vol. 26, no. 4, Jun. 2016, Art. no. 5201704.
[16] K. Hirata, T. Yamamoto, T. Yamaguchi, Y. Kawase, and Y. Hasegawa, "Dynamic analysis method of two-dimensional linear oscillatory actuator employing finite element method," *IEEE Trans. Magn.*, vol. 43, no. 4, pp. 1441–1444, Apr. 2007.
[17] J.-H. Lee, S.-H. Park, P.-J. Kim, D.-H. Park, and M.-S. Lim, "Two-dimensional FEA-based iron loss calculation method for linear oscillating actuator considering the circumferential segmented structure," *IEEE Trans. Magn.*, vol. 59, no. 11, Nov. 2023, Art. no. 8000605, doi: 10.1109/TMAG.2023.3275152.
[18] J.-H. Lee, S.-H. Park, D.-H. Park, J.-H. Jeong, and M.-S. Lim, "Deep transfer learning-based demagnetization analysis for linear oscillating actuator considering circumferential segmented structure," in *Proc. 2023 IEEE Transp. Electrific. Conf. Expo*, Chiang Mai, Thailand, 2023, pp. 1–5, doi: 10.1109/ITECAsia-Pacific59272.2023.10372241.
[19] G. J. Li, B. Ren, Z. Q. Zhu, M. P. Foster, and D. A. Stone, "Demagnetization withstand capability enhancement of surface mounted PM machines using stator modularity," *IEEE Trans. Ind. Appl.*, vol. 54, no. 2, pp. 1302–1311, Mar./Apr. 2018, doi: 10.1109/TIA.2017.2777922.
[20] Z.-X. Li, G.-L. Yang, Y.-M. Fan, and J.-H. Li, "Irreversible demagnetization mechanism of permanent magnets during electromagnetic buffering," *Defence Technol.*, vol. 17, no. 3, pp. 763–774, 2021, doi: 10.1016/j.dt.2020.05.005.
[21] P. Zhou, D. Lin, Y. Xiao, N. Lambert, and M. A. Rahman, "Temperature-dependent demagnetization model of permanent magnets for finite element analysis," *IEEE Trans. Magn.*, vol. 48, no. 2, pp. 1031–1034, Feb. 2012, doi: 10.1109/TMAG.2011.2172395.
[22] S. Doi, H. Sasaki, and H. Igarashi, "Multi-objective topology optimization of rotating machines using deep learning," *IEEE Trans. Magn.*, vol. 55, no. 6, Jun. 2019, Art. no. 7202605, doi: 10.1109/TMAG.2019.2899934.
[23] S.-H. Park, J.-W. Chin, K.-S. Cha, and M.-S. Lim, "Deep transfer learning-based sizing method of permanent magnet synchronous motors considering axial leakage flux," *IEEE Trans. Magn.*, vol. 58, no. 9, Sep. 2022, Art. no. 8206005, doi: 10.1109/TMAG.2022.3181804.
[24] K. Weiss, T. M. Khoshgoftaar, and D. D. Wang, "A survey of transfer learning," *J. Big Data*, vol. 3, no. 1, pp. 1–40, 2016.
[25] H. Xiong, J. Zhang, M. W. Degner, C. Rong, F. Liang, and W. Li, "Permanent-magnet demagnetization design and validation," *IEEE Trans. Ind. Appl.*, vol. 52, no. 4, pp. 2961–2970, Jul./Aug. 2016, doi: 10.1109/TIA.2016.2544739.
[26] M. Tahkola, J. Keränen, D. Sedov, M. F. Far, and J. Kortelainen, "Surrogate modeling of electrical machine torque using artificial neural networks," *IEEE Access*, vol. 8, pp. 220027–220045, 2020, doi: 10.1109/ACCESS.2020.3042834.
[27] F. Xiong et al., "Optimizing Latin hypercube design for sequential sampling of computer experiments," *Eng. Optim.*, vol. 41, no. 8, pp. 793–810, 2009.
[28] M. E. Johnson, M. L. Moore, and D. Ylvisaker, "Minimax and maximin distance designs," *J. Stat. Plan. Inference*, vol. 26, no. 2, pp. 131–148, 1990.
[29] S. Salman and X. Liu, "Overfitting mechanism and avoidance in deep neural networks," 2019, *arXiv:1901.06566*.
[30] M. M. Bejani and M. Ghatee, "A systematic review on overfitting control in shallow and deep neural networks," *Artif. Intell. Rev.*, vol. 54, no. 8, pp. 6391–6438, 2021.
[31] J. Qi, J. Du, S. M. Siniscalchi, X. Ma, and C.-H. Lee, "On mean absolute error for deep neural network based vector-to-vector regression," *IEEE Signal Process. Lett.*, vol. 27, pp. 1485–1489, 2020.

Ji-Hyeon Lee received the bachelor's degree in automotive engineering in 2021 from Hanyang University, Seoul, South Korea, where she is currently working toward the Ph.D. degree in automotive engineering.

Her research interests include the optimization, design, and AI-assisted acceleration of the design of electric machines.

Soo-Hwan Park (Member, IEEE) received the bachelor's degree in mechanical engineering and the Ph.D. degree in automotive engineering from Hanyang University, Seoul, South Korea, in 2014 and 2022, respectively.

From 2019 to 2020, he was with the Korea Institute of Industrial Technology, Daegu, South Korea. From 2022 to 2023, he was with the R&D Division of Hyundai Motor Company, Hwaseong, South Korea, as a Senior Research Engineer. Since 2023, he has been with the Department of Mechanical, Robotics, and Energy Engineering with Dongguk University, Seoul, where he is currently an Assistant Professor. His research interests include electromagnetic-mechanical analysis, design, and optimization of electric machines for automotive and robotics applications, and thermal management system for electric vehicles.

Du-Ha Park received the bachelor's degree in automotive engineering in 2022 from Hanyang University, Seoul, South Korea, where he is currently working toward the Ph.D. degree in automotive engineering. His research interests include electromagnetic field analysis, design, and optimization of electric machines.

Jae-Hoon Jeong received the B.S., M.S., and Ph.D. degrees in electrical engineering from Chungnam National University, Daejeon, South Korea, in 2008, 2013, and 2017, respectively. Since 2018, he has been a Chief Researcher with LG Electronics, Seoul. His research interests include the design, analysis, simulation, and implementation of linear and rotary motors, and linear compressors.

Myung-Seop Lim (Senior Member, IEEE) received the bachelor's degree in mechanical engineering and the master's and Ph.D. degrees in automotive engineering from Hanyang University, Seoul, South Korea, in 2012, 2014, and 2017, respectively. From 2017 to 2018, he was a Research Engineer with Hyundai Mobis, Yongin, South Korea. From 2018 to 2019, he was an Assistance Professor with Yeungnam University, Daegu, South Korea. Since 2019, he has been with Hanyang University, where he is currently an Assistant Professor. His research interests include electromagnetic field analysis and electric machinery for mechatronics systems, such as automotive and robot applications.